

# Observing the Sun with the Atacama Large Millimeter/submillimeter Array – from continuum to magnetic fields

Sven Wedemeyer<sup>1,2</sup> , Mikolaj Szydlarski<sup>1,2</sup>,  
Jaime de la Cruz Rodriguez<sup>3</sup> and Shahin Jafarzadeh<sup>1,2</sup>

<sup>1</sup>Rosseland Centre for Solar Physics, University of Oslo, Postboks 1029 Blindern, N-0315 Oslo, Norway

<sup>2</sup>Institute of Theoretical Astrophysics, University of Oslo, Postboks 1029 Blindern, N-0315 Oslo, Norway

<sup>3</sup>Institute for Solar Physics, Dept. of Astronomy, Stockholm University, Albanova University Center, SE-10691 Stockholm, Sweden

**Abstract.** The Atacama Large Millimeter/submillimeter Array offers regular observations of our Sun since 2016. After an extended period of further developing and optimizing the post-processing procedures, first scientific results are now produced. While the first observing cycles mostly provided mosaics and time series of continuum brightness temperature maps with a cadence of 1-2s, additional receiver bands and polarization capabilities will be offered in the future. Currently, polarization capabilities are offered for selected receiver bands but not yet for solar observing. An overview of the recent development, first scientific results and potential of solar magnetic field measurements with ALMA will be presented.

**Keywords.** Sun: atmosphere, Sun: chromosphere, Sun: radio radiation, radiation mechanisms: thermal, magnetic fields, polarization, techniques: interferometric

---

## 1. Introduction

The magnetic field plays an essential role in the structuring, dynamics, and energy balance in the atmospheres of solar-like stars. Measurements of the magnetic field in the upper atmospheric layers, however, are still challenging even for the Sun because of technical limitations in connection with the few currently available diagnostics. Common measurement techniques employ magnetically sensitive spectral lines that are formed in the chromosphere, such as the lines of singly ionized calcium (Ca II). These lines typically have only weak polarisation signals, which requires an instrument with high sensitivity. In addition, the meaningful interpretation of chromospheric spectral lines requires to properly take into account deviations from equilibrium conditions, in particular regarding non-local thermodynamic equilibrium (NLTE) and the ionization state of the chromospheric gas.

The continuum radiation at millimeter wavelengths is an alternative diagnostic tool for measuring magnetic fields in the atmosphere of the Sun and other stars. The Atacama Large Millimeter/Submillimeter Array (ALMA) has the potential of facilitating such measurements in the future. Regular continuum observations of the Sun with ALMA began in 2016. Full polarization capabilities are not yet available for solar observations but for non-solar targets for a few receiver bands. It should be emphasized that solar observations with ALMA are very different from observations of other targets because the Sun evolves on very short time scales and because the extent of the Sun is much

wider than ALMA's field-of-view so that the primary antenna beam is filled with complex emission. Consequently, developing robust procedures for calibration, imaging and further post-processing of regular (and also Commissioning and Science Verification) solar ALMA data was time-demanding. Now (in 2019), some first results are already produced and published (see, e.g. Bastian *et al.* 2017; Shimojo *et al.* 2017b; Yokoyama *et al.* 2018; Brajša *et al.* 2018; Jafarzadeh *et al.* 2019; Rodger *et al.* 2019; Selhorst *et al.* 2019; Nindos *et al.* 2018; Loukitcheva *et al.* 2019; Molnar *et al.* 2019; Wedemeyer *et al.* 2020. See also Wedemeyer *et al.* (2016)) for an overview of potential science cases with ALMA (see also Wedemeyer 2016; Bastian *et al.* 2018).

We focus here on ALMA's potential for measuring the magnetic field in the solar chromosphere since it is a challenging but important first step before the same can be attempted for other (and thus spatially unresolved) stars. In the following, we give a concise overview of ALMA's current observing capabilities relevant in this context (Sect. 2) and discuss ALMA's potential for future magnetic field measurements based on observations and numerical simulations (Sect. 3). A summary and outlook is provided in Sect. 4.

## 2. Observations so far

### 2.1. The Atacama Large Millimeter/Submillimeter Array (ALMA)

ALMA<sup>†</sup> is located on the Chajnantor plateau in the Chilean Andes close to San Pedro de Atacama at an altitude of 5100 m. The array consists of several components: The 12-m Array with 50 movable 12-m antennas and the Atacama Compact Array (ACA) with 12 antennas with 7 m diameter and 4 Total Power (TP) antennas with 12 m diameter for single dish observations. The ACA remains in a fixed compact configuration whereas the 12-m Array changes through different predefined configurations throughout the observing cycle. That way, ALMA can provide maximum baselines from a few hundred meters in a compact configuration to a maximum of 16 km in the most extended configuration.

ALMA is an aperture synthesis telescope with an angular resolution that corresponds to a telescope aperture equivalent to the longest baseline, i.e. the longest distance between two individual antennae. Each antenna pair in the array is sensitive to a certain spatial scale and orientation angle in the source image corresponding to one component in the spatial Fourier space. Each unique combination of two antennae in the array thus maps one Fourier component of the source image as determined by the length and orientation of the baseline with regard to the target position on the sky. The more unique Fourier components are measured, the better the sampling of the Fourier space and the better can the source image be reconstructed from the measured Fourier components. ALMA is therefore using a comparatively large number of antennae. The smaller antennae in the ACA have the advantage of providing shorter baselines as short as 8.5 m, which are otherwise impossible to obtain with 12-m antennae, and thus maps larger spatial scales inaccessible with the 12-m Array. The TP antennae, which are used for single-dish observations, measure the zero component in Fourier space and thus provide the absolute offset for the interferometric observations.

ALMA currently offers 8 different receiver bands for observations of non-solar targets covering a range from 84 GHz (3.6 mm) to 950 GHz (0.3 mm). The range will be eventually expanded to lower frequencies (35 GHz, 8.5 mm) once Band 1 and 2 become available. The receivers have two linear polarisation feeds with perpendicular orientation ( $X$  and  $Y$ ). ALMA offers both single and dual polarisation modes, providing the cross-correlation product  $\langle XX^* \rangle$  (with better spectral resolution) or  $\langle XX^* \rangle$  and  $\langle YY^* \rangle$  (with

<sup>†</sup> The ALMA project is an international partnership between Europe, North America, and East Asia in cooperation with the Republic of Chile and minor partners.

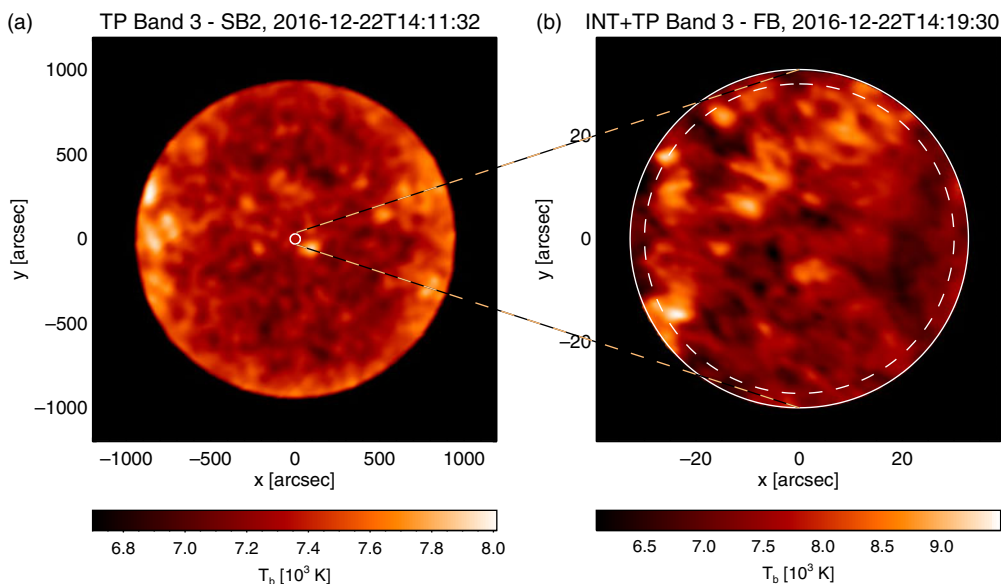


**Figure 1.** Examples of Band 3 observations of the Sun from the first regular solar observing campaign: **a)** Single-dish TP map and **b)** a (combined TP+) interferometric map. The dashed circle in the latter marks the single-dish beam, whereas the solid circles in both panels mark the chosen interferometric field-of-view. Please note that the whole Sun is shown in panel a whereas the map in panel b is only a small portion of the Sun.

better sensitivity), respectively. In full polarisation mode, all cross-correlation products are provided (see Sect. 2.3). The solar observing capabilities are described in Sect. 2.2.

## 2.2. ALMA's current capabilities for observing the Sun

Regular ALMA observations of the Sun were first offered in Cycle 4, which started in October 2016 with the first solar observations attempted in December 2016. Solar projects consist of interferometric observations either at a fixed target tracked for solar rotation or as a larger mosaic with up to 149 positions. In addition, the whole solar disk is scanned with single Total Power (TP) dishes in a double-circular motion in the course of a few minutes. As many of the fast TP scans are attempted at the same time (or close to) the interferometric observation. More technical details about the interferometric and the TP part are given by Shimojo *et al.* (2017a) and White *et al.* (2017), respectively. As example, a full-disk TP scan and a combined interferometric map, both obtained in Band 3, are shown in Fig. 1. The interferometric map has been combined (“feathered”) with the TP map and thus shows absolute brightness temperatures. Please see Wedemeyer *et al.* (2020) for details regarding the imaging and post-processing of this data set.

In Cycle 4 and 5, only the receiver bands 3 (3 mm) and 6 (1.3 mm) were offered but Band 7 (0.9 mm) followed in Cycle 7 (from October 2019, see Table 1). The interferometric data can be split into 4 sub-bands with a band-width of 2 GHz each and each sub-band can be split into 128 spectral channels each. The provided scripts for the first cycles do not split but combine all  $4 \times 128$  channels for the reconstruction of one “full-band” continuum image. This approach (multi-frequency synthesis) is chosen in order to maximize the spatial Fourier coverage and thus maximize the image fidelity. The full-disk TP scans are produced for all four sub-bands but cannot be further split into spectral channels.

The interferometric observations are typically carried out for a single pointing (following solar rotation) at a cadence of 1 s (2 s in Cycle 4) for a duration of  $\sim 10$  min before the

**Table 1.** Available solar observing modes: Receiver bands with central frequency  $\nu_{\text{LO1}}$  and corresponding wavelength  $\lambda$ , available array configurations with maximum baseline and when these capabilities were offered for the first time.

Band	$\nu_{\text{LO1}}$ [GHz]	$\lambda$ [mm]	First offered	Configuration (max. baseline)			
				1 (161 m)	2 (314 m)	3 (500 m)	4 (784 m)
3	100.0	3.00	Cycle 4	yes	yes	yes	since Cycle 7
6	239.0	1.25	Cycle 4	yes	yes	yes	no
7	346.6	0.86	Cycle 7	yes	yes	no	no

observation is interrupted for a 2-3 min intermediate calibration break. An observation often consists of 3-4 of these scans, resulting in a net observing time of up to  $\sim 40$  min. The field-of-view (FOV) is set by the primary beam of a single antenna or more precisely the chosen cut-off of the primary beam response. The resulting FOV is then typically  $60''$  for Band 3,  $25''$  for Band 6, and  $17''$  for Band 7. As mentioned above, larger areas on the Sun can be mapped with mosaics with up to 149 points, thus sacrificing the time domain to obtain one large map (see, e.g., Jafarzadeh *et al.* 2019, and references therein). The achievable angular resolution is determined by the observing wavelength, the longest available baseline (see Table 1), the position of the Sun on the sky, and in practice also the seeing conditions. According to the ALMA Technical Handbook (Cycle 7†), the resolution for Band 3 can be as low as  $1.42''$  (in configuration 3) and since Cycle 7 down to  $0.92''$  (in configuration 4), down to  $0.615''$  for Band 6, and down to  $0.666''$  for Band 7. For solar Band 3 observations so far, effective resolutions of down to  $1.4''$  for the minor axis of the synthesized beam are reported whereas the major axis is larger (on the order of  $\sim 2''$ ) and changes with the Sun moving across the sky.

Solar observations are typically carried out in dual linear polarization mode ( $\langle XX^* \rangle$ ,  $\langle YY^* \rangle$ ) although in principle the single-polarization ( $\langle XX^* \rangle$ ) mode is offered for solar observations, too. Using dual polarization mode has the advantage that  $\langle XX^* \rangle$  and  $\langle YY^* \rangle$  represent mostly independent measurements of the source, which can be exploited to suppress noise and improve the final image quality. Continuum images are therefore typically derived from the average of  $\langle XX^* \rangle$  and  $\langle YY^* \rangle$  under the assumption that there is no significant net linear polarisation and that averaging thus improves the image quality. ALMA offers no full polarisation for solar observations yet.

### 2.3. ALMA's current polarisation capabilities for (non-solar) targets

For non-solar targets, full polarisation capabilities are currently (Cycle 7) offered for single-pointing observations with the 12-m Array in bands 3, 4, 5, 6 and 7. All cross-correlation products are available for such observations:  $\langle XX^* \rangle$ ,  $\langle XY^* \rangle$ ,  $\langle YX^* \rangle$ ,  $\langle YY^* \rangle$  (or written as cross-correlation visibilities:  $V_{XX}$ ,  $V_{XY}$ ,  $V_{YX}$ ,  $V_{YY}$ ). Under ideal conditions, all Stokes components including linear and circular polarization states can be calculated from the visibilities:

$$I = \frac{1}{2}(V_{XX} + V_{YY}) \quad (2.1)$$

$$Q = \frac{1}{2}(V_{XX} - V_{YY}) \quad (2.2)$$

$$U = \frac{1}{2}(V_{XY} + V_{YX}) \quad (2.3)$$

$$V = \frac{1}{2i}(V_{XY} - V_{YX}) \quad (2.4)$$

† <https://almascience.nrao.edu/documents-and-tools/cycle7/alma-technical-handbook>

In practice, the separation into the two orthogonal polarization states ( $X$  and  $Y$ ) is not perfect and effects like instrumental polarization need to be corrected for. In addition, this correction and thus the calibration depends on the position within the primary beam. Consequently, only on-axis polarization is offered for Cycle 7, restricting the full polarization capabilities to the innermost parts of the primary beam, whereas off-axis polarization (i.e., position further away from the axis, i.e. away from the center of the FOV) is still under commissioning. Please see the ALMA Technical Handbook (Cycle 7†) for more details.

According to the ALMA Cycle 7 Proposer's Guide‡, the accuracy level of linear polarization imaging of a compact source on-axis (both in continuum and with full spectral resolution) is 0.1% ( $3\sigma$ , i.e. 3 times the systematic calibration uncertainty) within the inner third of the primary beam (i.e. within  $1/3$  of its FWHM). The corresponding accuracy for on-axis circular polarisation is currently 1.8% ( $3\sigma$ , 0.6% at  $1\sigma$ ). The field of view of the observations is limited to the inner one-third for linear polarisation observations and to the inner one-tenth of the primary beam FWHM for circular polarisation observations, respectively. Proper calibration of full polarization observations currently takes about three hours. Substantial efforts are being made to further develop and improve the accuracy of the full polarization mode and eventually offer it as a standard mode and for solar observations.

### 3. Prospects for measuring magnetic fields with ALMA

#### 3.1. Basic considerations

The radiation at millimeter wavelengths emitted from the Sun originates from its chromosphere. Non-thermal contributions such as gyrosynchrotron radiation are expected to be only significant during flares so that the solar millimeter radiation is of thermal nature in most situations. The solar atmosphere is permeated by magnetic field of varying strength, which is polarizing the thermal free-free radiation. A linearly polarized wave that is propagating through the chromosphere in the presence of magnetic fields is split into two components, namely the ordinary wave and extraordinary wave, also referred to as o-mode and x-mode, respectively. The absorption coefficient and thus the opacity  $\kappa$  is higher in the extraordinary mode than in the ordinary ( $\kappa_x > \kappa_o$ ), which results in a difference of the heights where the two modes become optically thick and thus from where the observed emission originates from. The x- and o-mode thus probe (slightly) different atmospheric layers with the difference of the formation heights of the x- and o-modes increasing with magnetic field strength. This effect produces an observable net circular polarisation

$$P = \frac{T_b^x - T_b^o}{T_b^x + T_b^o}, \quad (3.1)$$

which is thus connected to the observable (brightness) temperature difference between these two layers ( $T_b^x - T_b^o$ ). The average of the measurable brightness temperature for both modes gives the (continuum) brightness temperature:

$$T_{b,\text{cont}} = \frac{T_b^x + T_b^o}{2}. \quad (3.2)$$

Bogod & Gelfreikh (1980) and Grebinkij *et al.* (2000) developed a technique that exploits this effect and allows for deriving the longitudinal component  $B_1$  of the magnetic

† <https://almascience.nrao.edu/documents-and-tools/cycle7/alma-technical-handbook>

‡ <https://almascience.nrao.edu/documents-and-tools/cycle7/alma-proposers-guide>

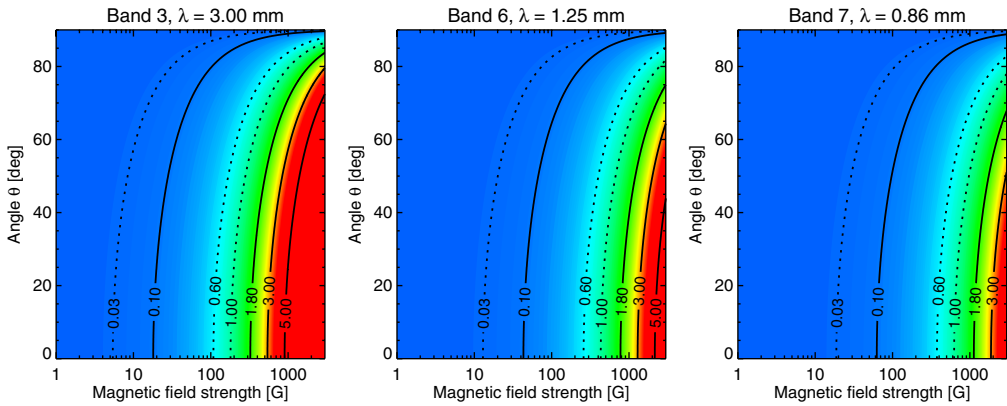


**Figure 2.** Estimate of the degree of circular polarisation for the central wavelengths of the ALMA bands 3, 6, and 7 as function of the magnetic field strength and the angle between the field orientation and the line of sight.

field from the observed degree of circular polarisation  $P$  and the slope  $\zeta = d(\log T_b)/d(\log \nu)$  of the brightness temperature spectrum  $T_b(\nu)$ . For the simple case of an optically thin, homogenous, and isothermal atmospheric gas (cf. Kundu 1965), the degree of circular polarization can then be approximated as

$$P(\%) \simeq 1.85 \times 10^{-3} \lambda \text{ (mm)} B \text{ (G)} \cos \theta \tag{3.3}$$

for an observing wavelength  $\lambda$  and for the longitudinal magnetic field component

$$B_1 = |\vec{B}| \cos \theta, \tag{3.4}$$

where  $\theta$  is the angle between the magnetic field vector  $\vec{B}$  and the line of sight. The resulting values are visualized for a wider range of field strengths and inclination angles for the central wavelengths of the ALMA bands 3, 6, and 7 in Fig. 2. According to this approximation, the degree of circular polarization is expected to be on the order of a few percent for a magnetic field strength of 1 kG as it occurs above sunspots (see, e.g., Wedemeyer *et al.* 2016, and references therein). More precisely, the approximation predicts values of up to  $P \approx 5.5\%$  for Band 3,  $2.3\%$  for Band 6, and  $1.6\%$  for Band 7, respectively. These numbers are in line with more realistic calculations by, e.g., Fleishman *et al.*, (in Wedemeyer *et al.* 2016) who derive  $|P|_{\text{max}} = 3.6\%$  for an Active Region at a frequency of 114.8 GHz ( $\lambda = 2.61$  mm, close to Band 3). The magnetic field strength in the Quiet Sun chromosphere is much lower and thus results in a correspondingly lower degree of circular polarization. Detailed modeling for the Quiet Sun chromosphere predicts values of only  $|P| \sim 0.05\%$  at  $\lambda = 1$  mm, which is clearly below the current detection limits mentioned in Sect. 2.3.

The same principle also offers a straightforward method for deriving the longitudinal component of the magnetic field from measurements of the circular polarization  $|P|$  and the (local) brightness temperature slope  $\zeta$  as

$$B_1 = |\vec{B}| \cos \theta = \frac{P \nu}{\zeta} (2.8 \times 10^6)^{-1} \text{ Hz}^{-1} \text{ (G)} \tag{3.5}$$

for the observing frequency  $\nu$ . The measured field component refers to an atmospheric height corresponding to the effective formation height at the observed frequency. In principle, the magnetic field  $B_1$  can be derived for different frequencies and thus for a corresponding range of heights in the solar atmosphere. Such measurements could allow for

reconstructing the magnetic field topology in the atmospheric layer probed with the chosen receiver band. See Loukitcheva *et al.* (2017) for a detailed evaluation of this method.

### 3.2. Model predictions for solar continuum polarisation

As already implied in Sect. 3.1, forward modelling can provide more realistic predictions for the polarization to be expected for observations of the Sun with ALMA. Even more importantly, such calculations can provide important input and tests for the development of more sensitive techniques that are applicable for weaker magnetic field strengths. Loukitcheva *et al.* (2017) calculate the degree of circular polarization based on a numerical model produced with the Bifrost code (Carlsson *et al.* 2016; Gudiksen *et al.* 2011) for a wavelength range covered by ALMA. The model is representative of an enhanced magnetic network region with a chromospheric magnetic field strength of up to  $\sim 100$  G. They derive values  $|P| < 0.15\%$  for a wavelength of 3.2 mm (Band 3) and only a few 0.01% for shorter wavelengths. Their polarisation signal would thus be lower than the current  $3\sigma$ -level of 1.8% (see Sect. 2.3), making the measurement of the magnetic field for the type of modelled region in Band 3 impossible given the current technical limitations. In Figs. 3–5, we present similar results calculated with the Advanced Radiative Transfer (ART) code (de la Cruz Rodriguez *et al.*, in prep.) for Band 3, 6, and 7, respectively. The model used for these calculations is a continuation of the simulation by Carlsson *et al.* (2016) with a newer version of the Bifrost code. The brightness temperatures are shown for the x- and o-mode separately, which can be combined to the continuum brightness temperature  $T_b$  and the circular polarization  $P$  according to Eqns. 3.2 and 3.1. The central region at 10% of the primary beam FWHM is marked for each band, illustrating the small region that will be initially be usable for circular polarization measurements. For Band 3 (Fig. 3), values of up to  $|P|_{\max} = 0.18\%$  are found for this particular model snapshot but most pixels exhibit much lower values as can be seen from the corresponding distribution in Fig. 6b. The same is true for the other two bands but the values decrease with wavelength. For Band 6 and 7, we find maximum values of  $|P|_{\max} = 0.09\%$  and  $|P|_{\max} = 0.07\%$ , respectively. Much of the simulated field of view and in particular the outer parts, which can be considered representative of Quiet Sun conditions, feature circular polarization signals that would be too weak even with a 10 times lower detection limit. However, the initial measurements will be confined to a small sub-region (on-axis) that even in Band 3 is just large enough to enclose one of the simulated magnetic patches. Such measurements will therefore require very accurate pointing and tracking of the solar rotation. The magnetic field measuring technique discussed in Sect. 3.1 (cf. Loukitcheva *et al.* 2017) might be improved by exploiting the fact that the circular polarisation can in principle be measured at several frequencies across the employed receiver band and thus at slightly different atmospheric heights. The resulting increased number of data points as input for data inversion codes might allow for lowering the effective detection limit to well below the  $3\sigma$  level. More numerical studies are needed in this regard.

### 3.3. Continuum polarisation from solar observations

As mentioned above, full polarization capabilities are not yet offered for solar observations. The data can nonetheless be split into the  $\langle XX^* \rangle$  and  $\langle YY^* \rangle$  cross-correlation products and used to construct images from on the corresponding visibilities separately. As we will show below, this procedure is still tentative and the resulting images must be interpreted with caution. The resulting maps in Fig. 7a and b are at first glance very similar. That is expected under the assumption that the mapped radiation from the chromosphere has no substantial linear polarization. The sum of the two maps or more precisely  $\frac{1}{2}(V_{XX} + V_{YY})$  (see Fig. 7c) should provide Stokes I (see Eq. 2.1) and is indeed

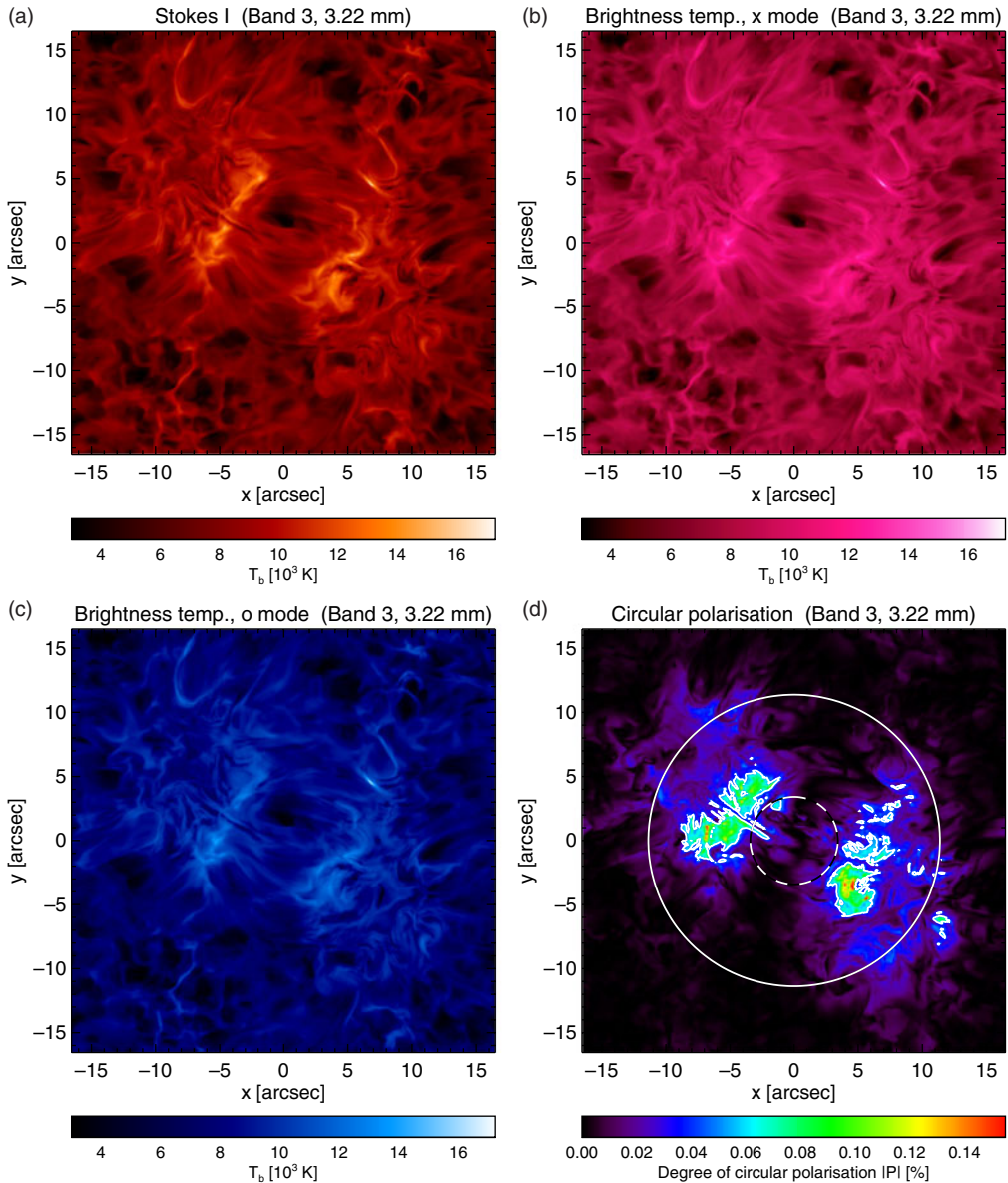


**Figure 3.** Results of a radiative transfer calculation with ART for a selected time step of the 3D numerical simulation. **a)** Continuum brightness temperature (Stokes I) for Band 3. **b)** Extraordinary mode (x-mode). **c)** Ordinary mode (o-mode). **d)** Absolute degree of circular polarisation  $|P|$  in percent. The white contour mark the  $|P| = 0.05\%$  level. The circles in panel d mark the FOV for 1/3 (white solid) and 0.1 (black-white dashed) times the width of the primary beam in Band 3.

very close to the continuum brightness temperature map derived from all visibilities for the same time step (similar to Fig. 1b but without the TP offset). The difference of the  $\langle XX^* \rangle$  and  $\langle YY^* \rangle$  maps (see Fig. 7d) should be zero if no significant linear polarization is expected. The difference can under that assumption be understood as brightness temperature uncertainty. The resulting value distribution can be well approximated with a Gaussian with  $\sigma = 15$  K (FWHM= 35 K) for the region with a diameter equivalent to the

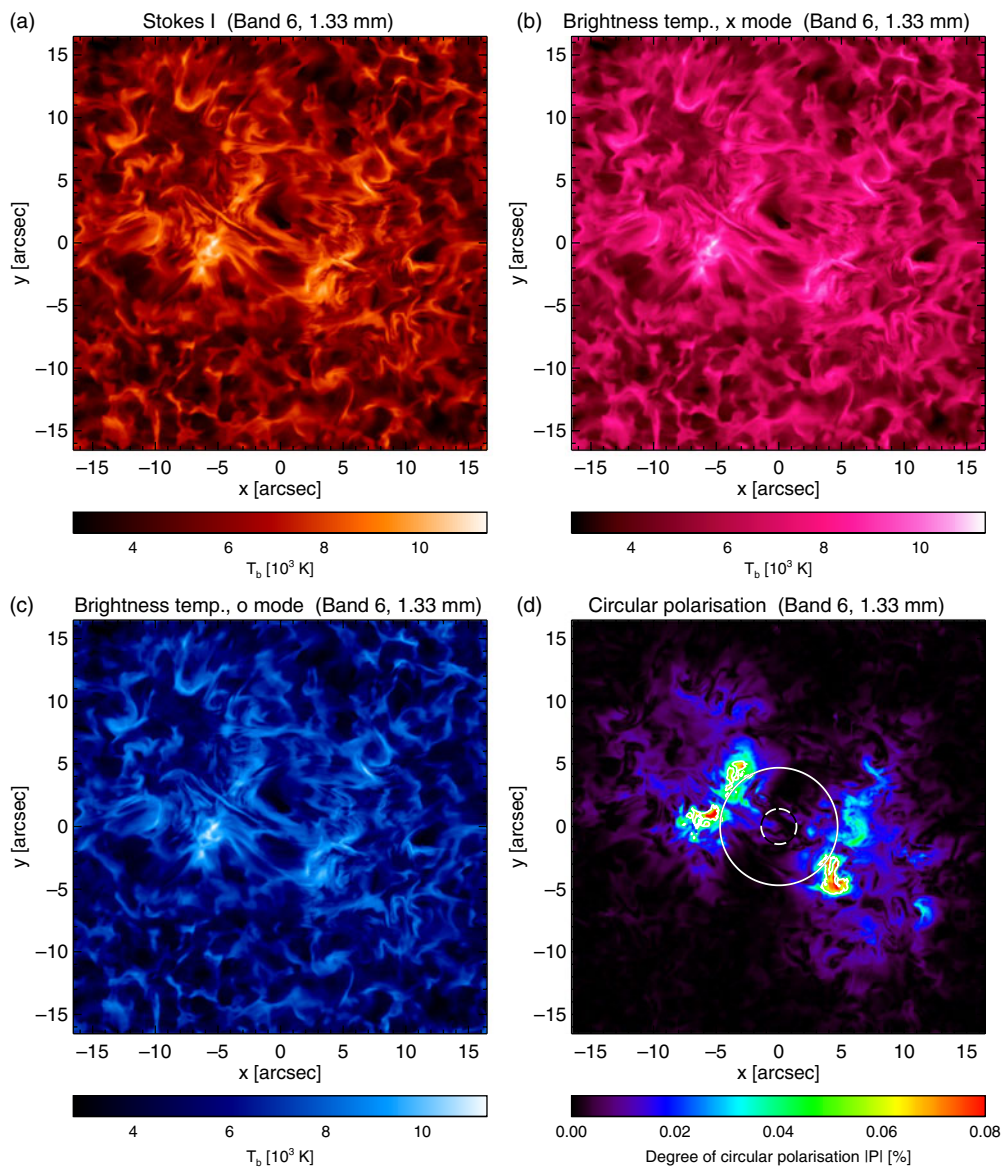


**Figure 4.** Results of a radiative transfer calculation with ART for a selected time step of the 3D numerical simulation. **a)** Continuum brightness temperature (Stokes I) for Band 6. **b)** Extraordinary mode (x-mode). **c)** Ordinary mode (o-mode). **d)** Absolute degree of circular polarisation  $|P|$  in percent. The white contour mark the  $|P| = 0.05\%$  level. The circles in panel d mark the FOV for  $1/3$  (white solid) and  $0.1$  (black-white dashed) times the width of the primary beam in Band 6.

primary beam FWHM (blue-white dashed circle in Fig. 7d) and  $\sigma = 9$  K (FWHM= 20 K) for the inner region with one third of that diameter (red-white dashed circle in Fig. 7d). Averaging over ten consecutive time steps does not change these numbers significantly.

In principle, the degree of linear polarization can be derived from the Stokes components as

$$L = \frac{\sqrt{Q^2 + U^2}}{I} . \quad (3.6)$$

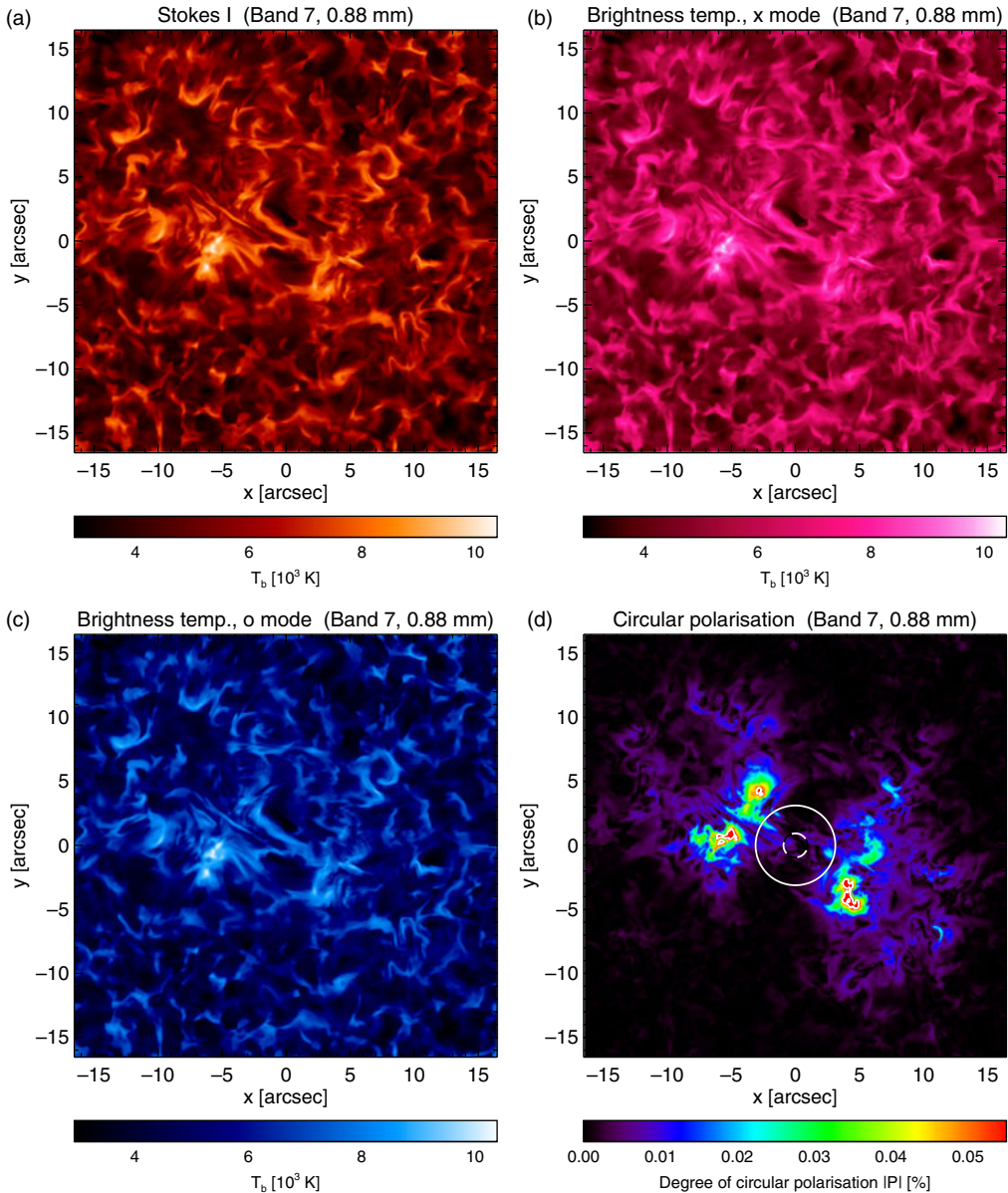


**Figure 5.** Results of a radiative transfer calculation with ART for a selected time step of the 3D numerical simulation. **a)** Continuum brightness temperature (Stokes I) for Band 7. **b)** Extraordinary mode (x-mode). **c)** Ordinary mode (o-mode). **d)** Absolute degree of circular polarisation  $|P|$  in percent. The white contour mark the  $|P| = 0.05\%$  level. The circles in panel d mark the FOV for  $1/3$  (white solid) and  $0.1$  (black-white dashed) times the width of the primary beam in Band 7.

The currently available  $\langle XX^* \rangle$  and  $\langle YY^* \rangle$  cross-correlation products for solar observations thus do not allow for deriving the full degree of linear polarization because the Stokes U component cannot be calculated. For now, only a lower limit of the linear polarization degree can be derived from  $(\langle XX^* \rangle - \langle YY^* \rangle) / (\langle XX^* \rangle + \langle YY^* \rangle)$  (see Fig. 7e). The distribution of the resulting values is shown for the two different regions at full and one third the primary beam FWHM. The distributions have a Gaussian core with

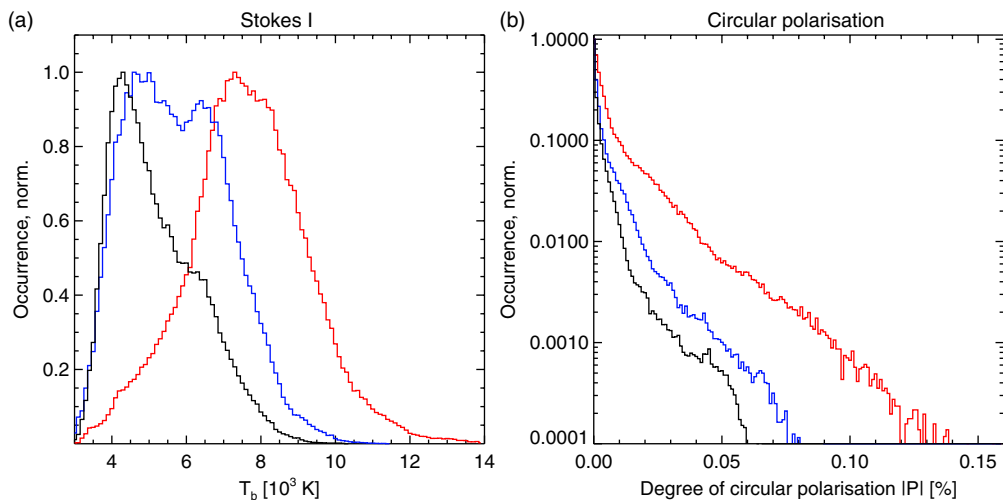


**Figure 6.** Histograms for **a)** the continuum brightness temperature (Stokes I) and **b)** absolute degree of circular polarisation  $|P|$  in percent for the Band 3, 6, and 7 maps (see Figs. 3–5), here colored red (Band 3), blue Band 6) and black (Band 7), respectively.

$\sigma \sim 4\%$  (FWHM = 9–11%), which is much more than expected based on measurements in other wavelength ranges (mostly lower in the atmosphere) and based on numerical simulations. For instance, Kuridze *et al.* (2018) derive a maximum degree of linear polarization of 1.5% from Ca II 854.2 nm observations of a flaring active region, which would be rather defining the maximum that can be expected at that wavelength. The linear polarization degree for the Quiet Sun target shown in Fig. 7 should be much lower. The maps shown in Fig. 7 have therefore most likely still large uncorrected contributions that hide the true linear polarization signal. We conclude that the linear polarisation can in principle be derived from ALMA observations of the Sun but that the calibration has yet to be improved and that a scientific analysis has to wait until the solar polarization capabilities are properly commissioned.

#### 4. Discussion and outlook

ALMA has started to produce first results regarding the thermal structure of the solar chromosphere and promises also to be developed into a promising tool for measuring magnetic fields in this enigmatic atmospheric layer. A solar polarisation test plan is developed and full solar polarisation (most likely starting with Band 3) will be commissioned and offered for regular observations in the future. Polarisation capabilities for further bands (most likely first Band 6, then Band 7) will follow. Based on the experience with ALMA observations of the Sun so far, it must be emphasized that solar observing is a non-standard mode and that consequently the development of adequate calibration and post-processing techniques for solar polarisation data and further improvements are necessary. These tasks will require significant efforts from the involved scientific community. The necessary development can and should be guided by forward modelling as presented here and already by, e.g., Loukitcheva *et al.* (2017), Loukitcheva (2020) and Nita *et al.* (2015) (see also references therein). The circular polarisation signals in Quiet Sun regions are expected to be typically smaller than 0.1% for the currently available receiver bands, whereas a few percent are expected for regions above sunspots. It is thus most promising to start solar magnetic field measurements with ALMA with sunspot observations in Band 3. Those observations will then help to further develop the proposed method in

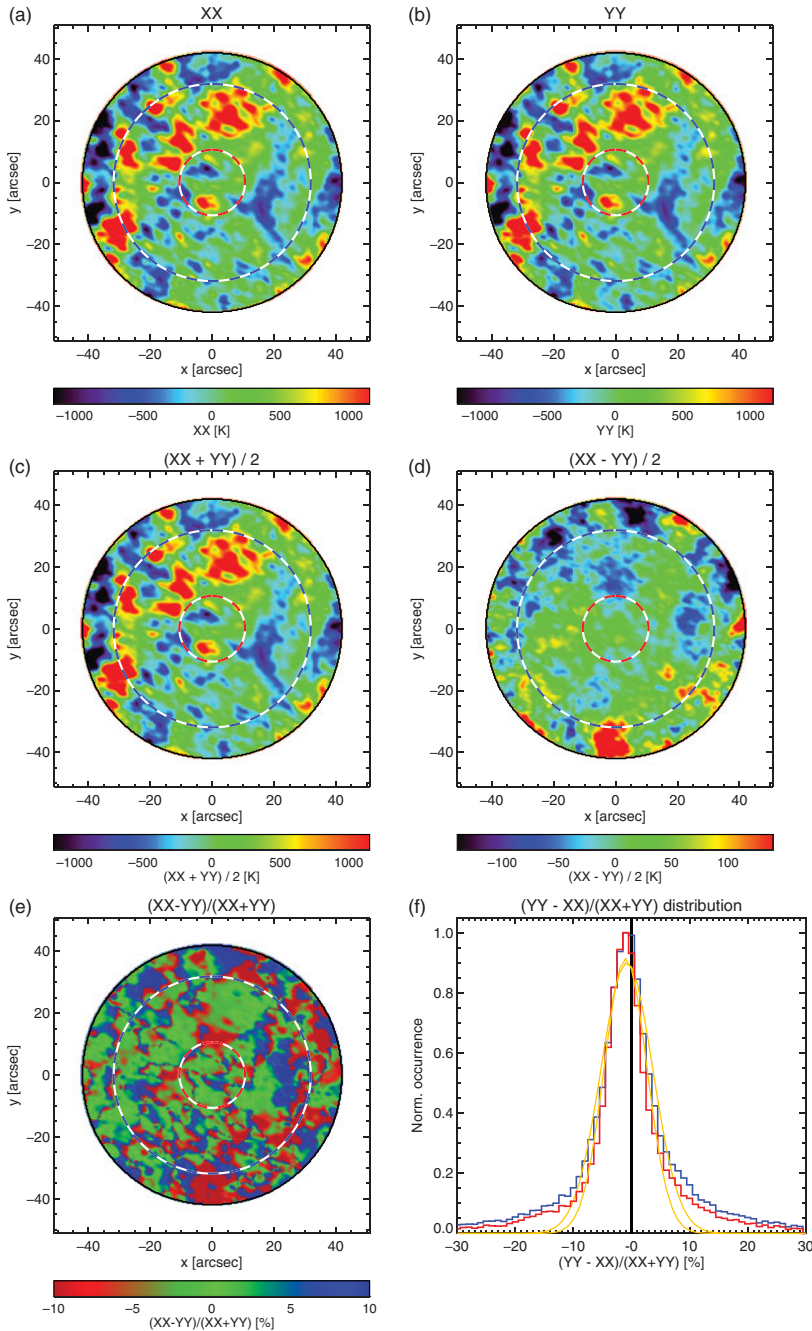


**Figure 7.** A solar Band 3 observation obtained on 2016-12-22 UT14:20:00 and split into the cross-correlation products **a)**  $\langle XX^* \rangle$  and **b)**  $\langle YY^* \rangle$ . Under ideal conditions, the combinations **c)**  $\frac{1}{2}(V_{XX} + V_{YY})$  and **d)**  $\frac{1}{2}(V_{XX} - V_{YY})$  would correspond to Stokes I and Q, respectively. **e)** The ratio of these two maps, which would correspond to a lower limit of the linear polarization degree under ideal conditions, is also shown as histogram in panel **f)** as blue line for the region defined by the primary beam FWHM (blue-white dashed circle in the maps) and as red line for the innermost region with a radius of 1/3 of the primary beam FWHM (red-white dashed circle in the maps). It must be emphasized that the results clearly show that a scientific analysis must wait until the polarization capabilities are commissioned.

view of the low expected levels of polarisation in comparison to the currently achievable accuracy with ALMA. Once reliable magnetic field measurements with ALMA become possible for the Sun, these results will help to interpret (spatially unresolved) ALMA observations of other stars.

## Acknowledgments

This work is supported by the SolarALMA project, which has received funding from the European Research Council (ERC) under the European Union's Horizon 2020 research and innovation programme (grant agreement No. 682462), and by the Research Council of Norway through its Centres of Excellence scheme, project number 262622. This paper makes use of the following ALMA data: ADS/JAO.ALMA#2016.1.00423.S. ALMA is a partnership of ESO (representing its member states), NSF (USA) and NINS (Japan), together with NRC(Canada), MOST and ASIAA (Taiwan), and KASI (Republic of Korea), in co-operation with the Republic of Chile. The Joint ALMA Observatory is operated by ESO, AUI/NRAO and NAOJ. We are grateful to the many colleagues who contributed to developing the solar observing modes for ALMA and for support from the ALMA Regional Centres. We acknowledge support from the Nordic ARC node based at the Onsala Space Observatory Swedish national infrastructure, funded through Swedish Research Council grant No 2017-00648, and collaboration with the Solar Simulations for the Atacama Large Millimeter Observatory Network (SSALMON, <http://www.ssalmon.uio.no>). The ISSI international team 387 "A New View of the Solar-stellar Connection with ALMA" was funded by the International Space Science Institute (ISSI, Bern, Switzerland). We thank Vasco Manuel de Jorge Henriques and Tobia Carozzi for helpful comments.

## References

- Bastian, T. S., Bárta, M., Brajša, R., *et al.* 2018, *The Messenger*, 171, 25
- Bastian, T. S., Chintzoglou, G., De Pontieu, B., *et al.* 2017, *Astrophys. J. Lett.*, 845, L19
- Bogod, V. M. & Gelfreikh, G. B. 1980, *Solar Phys.*, 67, 29
- Brajša, R., Sudar, D., Benz, A. O., *et al.* 2018, *A&A*, 613, A17
- Carlsson, M., Hansteen, V. H., Gudiksen, B. V., Leenaarts, J., & De Pontieu, B. 2016, *A&A*, 585, A4
- de la Cruz Rodriguez, J., Szydlarski, M., Wedemeyer, S., & *et al.* in prep., *The Advanced Radiative Transfer code*
- Grebinskij, A., Bogod, V., Gelfreikh, G., *et al.* 2000, *A&AS*, 144, 169
- Gudiksen, B. V., Carlsson, M., Hansteen, V. H., *et al.* 2011, *A&A*, 531, A154+
- Jafarzadeh, S., Wedemeyer, S., Szydlarski, M., *et al.* 2019, *A&A*, 622, A150
- Kundu, M. R. 1965, *Solar radio astronomy* (Interscience Publication, New York)
- Kuridze, D., Henriques, V. M. J., Mathioudakis, M., *et al.* 2018, *Astrophys. J.*, 860, 10
- Loukitcheva, M., White, S. M., Solanki, S. K., Fleishman, G. D., & Carlsson, M. 2017, *A&A*, 601, A43
- Loukitcheva, M. A., White, S. M., & Solanki, S. K. 2019, *Astrophys. J. Lett.*, 877, L26
- Loukitcheva, M. 2020, *Front. Astron. Space Sci.*, 11 August 2020 (<https://doi.org/10.3389/fspas.2020.00045>)
- Molnar, M. E., Reardon, K. P., Chai, Y., *et al.* 2019, *Astrophys. J.*, 881, 99
- Nindos, A., Alissandrakis, C. E., Bastian, T. S., *et al.* 2018, *A&A*, 619, L6
- Nita, G. M., Fleishman, G. D., Kuznetsov, A. A., Kontar, E. P., & Gary, D. E. 2015, *Astrophys. J.*, 799, 236
- Rodger, A. S., Labrosse, N., Wedemeyer, S., *et al.* 2019, *Astrophys. J.*, 875, 163
- Selhorst, C. L., Simões, P. J. A., Brajša, R., *et al.* 2019, *Astrophys. J.*, 871, 45
- Shimojo, M., Bastian, T. S., Hales, A. S., *et al.* 2017a, *Solar Phys.*, 292, #87

- Shimojo, M., Hudson, H. S., White, S. M., Bastian, T. S., & Iwai, K. 2017b, *Astrophys. J. Lett.*, 841, L5
- Wedemeyer, S. 2016, *The Messenger*, 163, 15
- Wedemeyer, S., Bastian, T., Brajša, R., *et al.* 2016, *Space Sci. Rev.*, 200, 1
- Wedemeyer, S., Szydlarski, M., Jafarzadeh, S., *et al.* 2020, *A&A*, 635, A71
- White, S. M., Iwai, K., Phillips, N. M., *et al.* 2017, *Solar Phys.*, 292, #88
- Yokoyama, T., Shimojo, M., Okamoto, T. J., & Iijima, H. 2018, *Astrophys. J.*, 863, 96

## Discussion

CALLY: Does your data processing to remove jumping in the images also delete real oscillation data?

WEDEMEYER: We have been very careful with developing the processing routines and indeed investigated the oscillation properties. The results will be published in a forthcoming article. I would say that it is most important to gain confidence in the processed data first. After that, we can certainly see if the processing routines can be improved even further to make sure that the oscillation properties of the observations are preserved.

BOMMIER: My question is very naive. Is it possible to observe/measure the solar corona? If spectral lines and polarization can be measured, this wavelength range (mm) is the most favorable to measure the coronal field by Zeeman effect in spectral lines. This field remains unknown up to day.

WEDEMEYER: As I showed during my presentation, there seem to be weak imprints of the corona in the ALMA Band 3 continuum maps but it is not clear yet how much can be learned about the corona from that. Unfortunately, spectral lines have not been detected yet in the available solar ALMA observations. Only after and if we have found suitable spectral lines, we can evaluate if measuring the coronal magnetic field with ALMA is possible.